Journal of the Optical Society of America B
OPTICAL PHYSICS

Broadband and wide angle nonreciprocal thermal emission from Weyl semimetal structures

ANDREW BUTLER[1] AND CHRISTOS ARGYROPOULOS[2,*]

[1]Department of Electrical and Computer Engineering, University of Nebraska-Lincoln, Lincoln, Nebraska 68588, USA
[2]Department of Electrical Engineering, The Pennsylvania State University, University Park, Pennsylvania 16803, USA
*cfa5361@psu.edu

Received 16 May 2023; revised 28 June 2023; accepted 6 July 2023; posted 6 July 2023; published 20 July 2023

Nonreciprocal thermal emission is a cutting-edge technology that enables fundamental control over thermal radiation and has exciting applications in thermal energy harvesting. However, thus far one of the foremost challenges is making nonreciprocal emission operate over a broad wavelength range and for multiple angles. In this work, we solve this outstanding problem by proposing three different types of structures that always utilize only one Weyl semimetal (WSM) thin film combined with one or two additional dielectric or metallic layers and terminated by a metallic substrate. First, a tradeoff relationship between the magnitude and bandwidth of the thermal nonreciprocity contrast is established based on the thickness of the WSM film. Then, the bandwidth broadening effect is demonstrated via the insertion of a dielectric spacer layer that can also be fine-tuned by varying its thickness. Finally, further control on the resulting strong nonreciprocal thermal radiation is demonstrated by the addition of a thin metallic layer in the proposed few layer designs. The presented composite structures work for a broad frequency range and for multiple emission angles, resulting in highly advantageous properties for various nonreciprocal thermal radiation applications. Moreover, the proposed designs do not require any patterning and can be experimentally realized by simple deposition fabrication methods. They are expected to aid in the creation of broadband nonreciprocal thermal emitters that can find applications in new energy harvesting devices.

https://doi.org/10.1364/JOSAB.495725

1. INTRODUCTION

Thermal radiation is a fundamental natural phenomenon where light is spontaneously emitted from an object due to increased heating [1,2]. The photonic engineering of thermal radiation has enabled exciting and novel applications such as passive radiative cooling [3–5] and thermophotovoltaics [6,7]. Typically, thermal radiation is governed by Kirchhoff's law, which equates the thermal emissivity of an object with its absorptance when it is in thermal equilibrium. However, emerging materials with asymmetric permittivity tensors can break Kirchhoff's law, resulting in nonreciprocal thermal radiation [8]. Such nonreciprocal thermal emitters will have exciting applications in energy harvesting devices since they can drastically improve their efficiency by reducing energy loss to unwanted thermal radiation channels [9,10].

One of the most common ways to design nonreciprocal thermal emitters is by using magneto-optical materials that utilize an external magnetic field to create asymmetric off-diagonal components in the material's permittivity tensor [11,12]. Indium Arsenide (InAs) is a common magneto-optical material used in thermal radiation applications. Nonreciprocal absorption and emissivity have been theoretically predicted in InAs gratings when an external magnetic field is applied [8]. Another recently introduced theoretical design was able to reduce the required magnetic field strength to break reciprocity by using a silicon (Si) grating coupled to an InAs layer [13]. In terms of experiments, nonreciprocal absorption in the mid-infrared (mid-IR) has just been demonstrated by using a similar structure of a silicon carbide (SiC) grating on a InAs layer [14]. In addition, another relevant design theoretically proposed tunable nonreciprocity by introducing a graphene monolayer between a metallic grating and InAs layer [15]. Highly directional emission was also achieved by using an InAs grating embedded inside an aluminum (Al) cavity, producing strong nonreciprocity at angles extremely close to the normal direction [16]. An alternative magneto-optical material is indium antimonide (InSb), which was used to achieve broadband nonreciprocal thermal emission in a recent work [17]. An unfortunate drawback of all these designs, however, is the requirement of an external magnetic field which can severely limit their realistic application, since magnets are bulky, expensive, and lossy. Finally, an alternative theoretical approach to achieving nonreciprocal thermal emission has been proposed based on modulating in time the graphene's conductivity [18,19], which consists of another way to break reciprocity by applying external bias [20]. While it is an interesting idea, it is very challenging to achieve

the rapid time-modulation of graphene properties experimentally. Note that most aforementioned designs are based on the diffraction mechanism due to the utilization of gratings that inherently limit the bandwidth response of nonreciprocal thermal emission.

Lately, increased attention has been dedicated to Weyl semimetals (WSMs), which are materials with inherent asymmetric permittivity tensors [21]. The intrinsic asymmetric optical constants of WSMs are an attractive option for achieving nonreciprocal radiation without the limitations stemming from external biases, such as magnets and time modulation. Gratings composed of WSMs have been theoretically shown to produce nonreciprocal emissivity [22]. Violation of Kirchhoff's Law of thermal radiation has been shown in WSM thin films over a metallic substrate [23]. Multilayer photonic crystal designs using many WSMs layers have also been proposed to enhance nonreciprocity [24,25]. Moreover, optical Tamm states formed by multilayer WSM-based photonic crystals have been shown to enhance nonreciprocity [26,27]. One problem pervading all the aforementioned works is that the narrow-band nonreciprocity is mainly due to the used grating and photonic crystal designs and works only for a specific range of angles. In addition, complex nanopatterning or multilayer deposition methods need to be employed to achieve these types of structures [28] that are very difficult to implement in practice, especially when emerging materials such as WSM are employed that are still immature in terms of fabrication. Hence, one of the foremost challenges is designing WSM-based structures that achieve broadband and omnidirectional nonreciprocal thermal emission that can be realized with as simple a fabrication process as possible. One recent work theoretically proposed a Si grating over a WSM thin film and metallic substrate to achieve broad angled nonreciprocal emission in the infrared [29]. However, the results of this work are still relatively narrowband and are based on analytical modeling as opposed to the usually more accurate full-wave computational simulations.

In this work, we propose three relatively simple-to-fabricate designs, which always consist of of one WSM thin film atop a metallic substrate and are combined with either one or two dielectric or metal spacer layers. First, we show that the thickness of the single WSM film affects the thermal nonreciprocity contrast bandwidth that can be extended to a very large range in the mid-IR spectrum. Next, we introduce a dielectric spacer layer and establish a tradeoff relationship between the obtained broad bandwidth and the nonreciprocity contrast magnitude. Finally, we demonstrate that the broadening effect can be tuned in the mid-IR range and beyond by using a thin metallic layer inserted between the WSM film and the dielectric spacer layer. All the presented designs lead to significant thermal nonreciprocity contrast values obtained over a broad wavelength range and for a wide range of emission angles. The proposed relatively omnidirectional and broadband nonreciprocity can be experimentally realized by simple deposition fabrication methods. The obtained structures are expected to have various new applications in emerging thermal energy harvesting devices.

2. RESULTS

The proposed structures are always made of one WSM layer, as illustrated in Fig. 1. The first design in Fig. 1(a) is a monolayer structure consisting simply of a WSM thin film of thickness t_{WSM} atop a metallic substrate. This design works as an extremely simple nonreciprocal emitter. In our work, tungsten (W) is always used as the substrate metallic material, which can also sustain high heating. In the second design in Fig. 1(b), a dielectric spacer layer composed of germanium (Ge) with thickness t_{Ge} is introduced between the WSM layer and the substrate creating a bilayer structure. The addition of the spacer layer causes a band-broadening effect, improving the bandwidth of the nonreciprocal emission. Moreover, the choice of Ge was mainly employed due to its low losses at the mid-IR range compared to oxide materials that exhibit high losses in this wavelength range due to the excitation of phonon–polariton resonances [30]. Finally, in the design of Fig. 1(c), an additional very thin W layer of thickness t_{W} is added between the WSM and dielectric layer creating a trilayer structure. This metallic layer enables further tuning of the bandwidth and magnitude of the nonreciprocal response. Figure 1(d) illustrates a three-dimensional (3D) schematic of the WSM designs and depicts the dimensions of each layer.

The reflectance, absorptance, and emissivity spectra of the proposed designs are accurately calculated based on full-wave simulations using the commercial finite element method (FEM) software COMSOL Multiphysics. Transverse magnetic (TM) polarized plane waves are incident upon the proposed structures at an angle θ. The absorbed and reflected power is calculated for various wavelengths and incident angles to determine the absorptance and reflectance values, respectively. Periodic conditions are utilized on the side boundaries of the simulation domain. Tungsten and germanium are modeled using their experimentally derived frequency dependent complex valued optical constants [31,32], where losses are also taken into full account. The permittivity tensor of the WSM is given by the following Eq. (1) [33]:

$$\varepsilon_{\mathrm{WSM}} = \begin{bmatrix} \varepsilon_d & j\varepsilon_a & 0 \\ -j\varepsilon_a & \varepsilon_d & 0 \\ 0 & 0 & \varepsilon_d \end{bmatrix}, \tag{1}$$

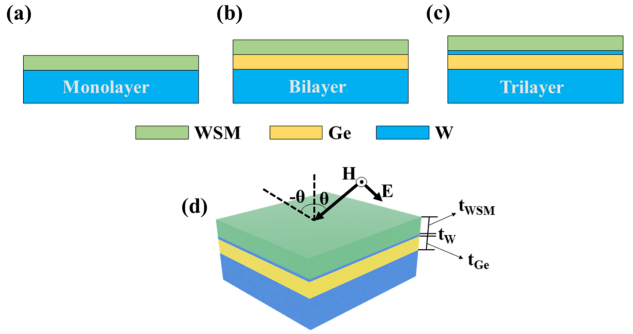

Fig. 1. (a)–(c) Schematics of the monolayer, bilayer, and trilayer WSM nonreciprocal thermal emitters. (d) 3D schematic of the structure with the thickness dimension of each layer is also illustrated. The oblique incidence plane wave illumination is also depicted.

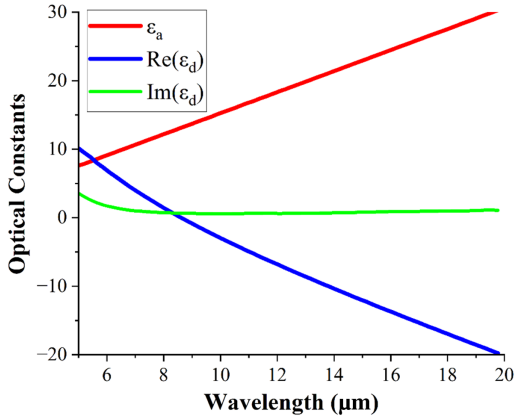

Fig. 2. Components of the WSM permittivity tensor versus the wavelength. Values taken from [35].

where ε_d represents the complex diagonal components of the permittivity tensor, and ε_a represents the off-diagonal asymmetric components that lead to a nonreciprocal response. Note that all presented designs work for TM polarized light excitation since both magneto-optical materials and WSMs can have asymmetric off-diagonal permittivity components given by Eq. (1) only for this type of polarization. This poses some limitations for incoherent radiation emission but can be useful in various applications that require polarized thermal radiation, similar to the broadband directional thermal emission that has recently been experimentally demonstrated only for TM polarized light [34]. The components of the WSM permittivity tensor are plotted in Fig. 2 [35].

We begin our investigation by considering the simple single layer design presented in Fig. 1(a). The reflectance as a function of wavelength and angle of incidence $R(\lambda, \theta)$ is calculated. From the reflectance, the absorptance $A(\lambda, \theta)$ and emissivity $E(\lambda, \theta)$ can be computed by using Eqs. (2) and (3) [23],

$$A(\lambda, \theta) = 1 - R(\lambda, \theta), \tag{2}$$

$$E(\lambda, \theta) = 1 - R(\lambda, -\theta). \tag{3}$$

The nonreciprocity contrast metric of the structure (η) is then defined as

$$\eta(\lambda, \theta) = |A(\lambda, \theta) - E(\lambda, \theta)|. \tag{4}$$

This metric should be equal to zero for ordinary reciprocal structures at thermal equilibrium when computed for any wavelength and angle of incidence. However, this is not the case in the current nonreciprocal designs. In particular, Figs. 3(a) and 3(b) show the nonreciprocity contrast metric η as a function of the angle and wavelength for the monolayer structure [Fig. 1(a)] with $t_{WSM} = 300$ nm and $t_{WSM} = 500$ nm, respectively. Furthermore, Figs. 3(c) and 3(d) demonstrate the quantity $1 - R(\lambda, \theta)$ of the same structures as a function of the angle and wavelength for positive and negative incident angles. Since emissivity is calculated based on the reflectance for negative angles and absorptance is calculated with positive angles, these plots illustrate both the emissivity and absorptance. In addition, these plots should have been symmetric if the reciprocity was not broken. The nonreciprocity contrast η reaches a peak value of ~0.8 for a WSM thickness of 300 nm. The peak value of η is reduced to ~0.6 when the WSM thickness is increased to 500 nm with the advantage that the nonreciprocity remains high over a broader wavelength range. In both cases, the nonreciprocity metric is bifurcated into two bands. Figures 3(c) and 3(d) illustrate the reason for this bifurcation. At lower wavelengths, the absorptance (computed for $\theta > 0$) is high, while at higher wavelengths the emissivity (calculated for $\theta < 0$) is high. At $\theta = 0$, the structure switches from high absorptance to high emissivity and the nonreciprocity metric becomes zero, as can be seen in Figs. 3(a) and 3(b), i.e., reciprocal operation. In these designs, we limit ourselves to considering only WSM layers with

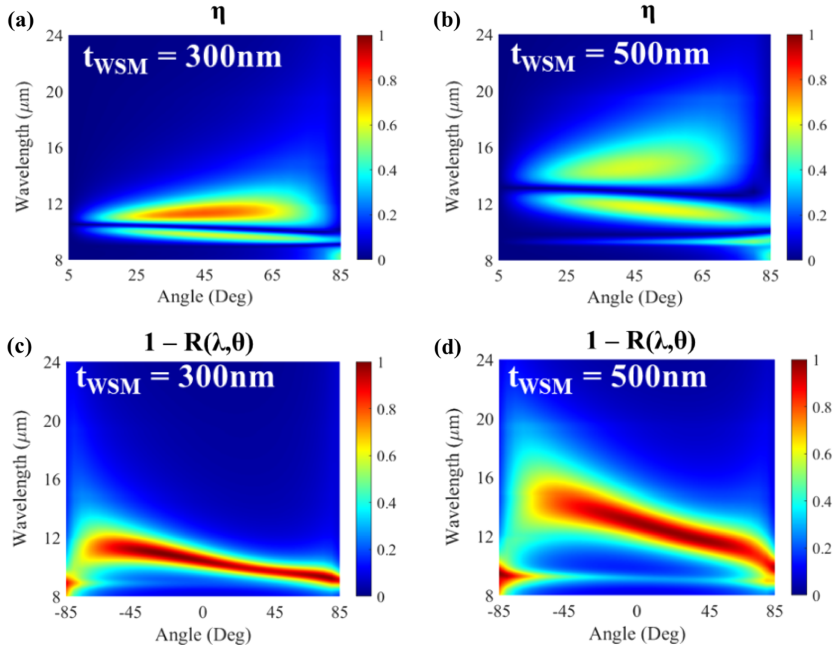

Fig. 3. (a),(b) Nonreciprocity contrast metric and (c),(d) $1 - R(\lambda, \theta)$ quantity versus the angle and the wavelength for the monolayer structure shown in Fig. 1(a) with the WSM layer thicknesses of 300 nm and 500 nm, respectively.

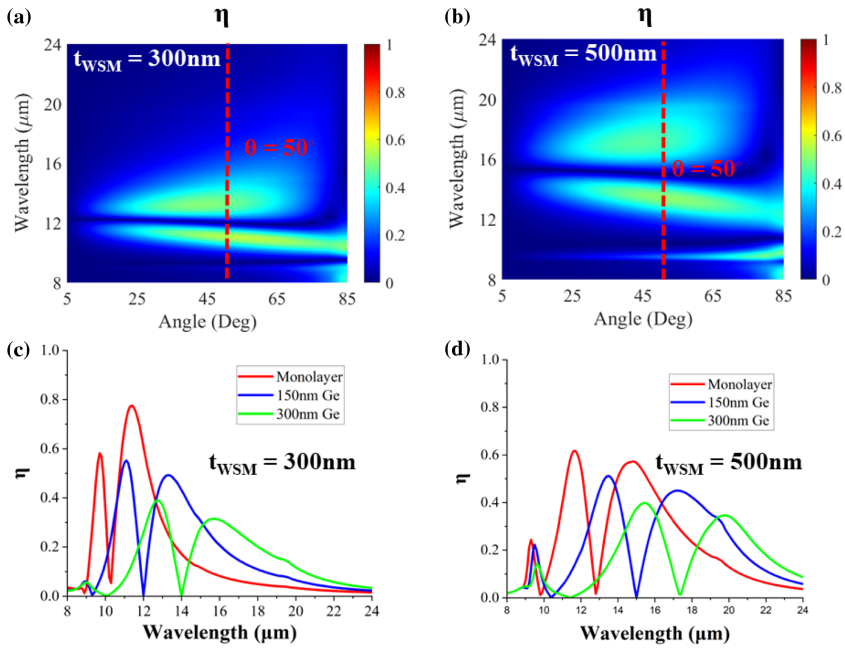

Fig. 4. (a),(b) Nonreciprocity contrast metric versus the angle and the wavelength for the bilayer structure shown in Fig. 1(b) with fixed t_{Ge} = 150 nm and WSM layer thicknesses of 300 nm and 500 nm, respectively. (c),(d) Line plots of the nonreciprocity contrast metric at fixed $\theta = 50°$ when t_{Ge} is ranging from 0 nm (monolayer design) to 300 nm (bilayer design) and the WSM layer thicknesses are equal to 300 nm and 500 nm, respectively.

thicknesses of a few hundred nanometers which is more feasible for fabrication compared to the several micron-thick films used in [23].

Figure 3 clearly demonstrates that the bandwidth of the nonreciprocity increases with the thickness of the WSM layer. However, there is a small tradeoff relationship between the bandwidth and the magnitude of the nonreciprocity contrast, which led us to consider a maximum limit of a 500-nm-thick WSM layer. Next, we study the bilayer structure illustrated in Fig. 1(b), where a thin layer of Ge is inserted between the WSM layer and the metallic substrate. This extra dielectric layer creates an additional cavity that is expected to lead to increased bandwidth in absorption or emission. Figures 4(a) and 4(b) show the nonreciprocity metric as a function of the angle and wavelength for fixed $t_{Ge} = 150$ nm combined with $t_{WSM} = 300$ nm or $t_{WSM} = 500$ nm, respectively. While the magnitude of the nonreciprocity contrast is reduced, the bandwidth for both cases is substantially increased compared to the monolayer designs with results depicted before in Fig. 3. This broadening effect is further illustrated in Figs. 4(c) and 4(d), where the nonreciprocity metric for both WSM thicknesses is plotted when the incident angle is fixed to $\theta = 50°$ but for two different thicknesses of the Ge spacer layer. As the Ge thickness increases, the nonreciprocity becomes broader, spreading to a substantial part of the IR spectrum. However, the tradeoff relationship between the bandwidth and the nonreciprocity contrast magnitude turns out to be even more pronounced. This enables tuning the nonreciprocal thermal emission of the proposed structure just by changing the Ge layer thickness.

The cause of the broadening effect in the nonreciprocity can be further understood by examining the induced electric field distribution in the presented structures. Towards this goal, Figs. 5(a) and 5(b) depict the computed electric field enhancement induced at the monolayer structure of Fig. 1(a) for $\theta = -45°$ and $\theta = +45°$ at $\lambda = 11.3$ μm, where the nonreciprocity is the strongest. Here, we consider fixed $t_{WSM} = 300$ nm. In both cases, the fields decay inside the WSM layer. However, the field enhancement is substantially stronger inside the WSM layer when the light is incident from the negative direction. Figures 5(c) and 5(d) demonstrate the induced field enhancement in the bilayer structure when the Ge spacer layer is introduced below the WSM layer. In this case, maximum nonreciprocity occurs at $\theta = \pm 55°$ and $\lambda = 11$ μm. Here, the induced field enhancement is low inside the WSM layer and negligible within the Ge spacer when the negative direction is considered. However, the induced field enhancement in the

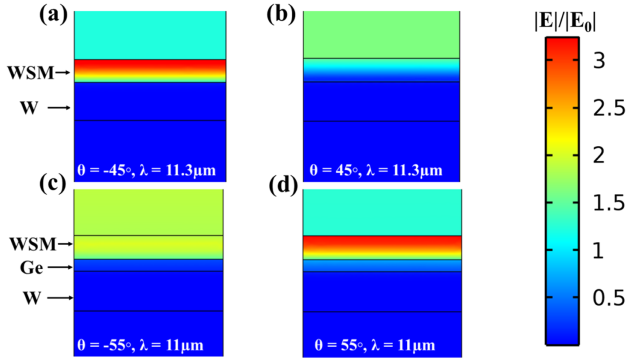

Fig. 5. (a),(b) Induced electric field enhancement distribution through the monolayer structure shown in Fig. 1(a) for $\theta = \pm 45°$ and $\lambda = 11.3$ μm. (c),(d) Induced electric field enhancement distribution through the bilayer structure depicted in Fig. 1(b) for $\theta = \pm 55°$ and $\lambda = 11$ μm.

WSM is much stronger and also leaks within the Ge layer in the case of positive direction illumination. These results clearly demonstrate the nonreciprocal dynamics that lead to dissimilar field enhancement from different direction illumination.

The thermal nonreciprocity of the structures can be further tuned through the addition of an ultrathin tungsten layer, resulting in the trilayer design presented in Fig. 1(c). Figures 6(a) and 6(b) demonstrate the computed nonreciprocity contrast metric of this structure for fixed $t_W = 5$ nm, $t_{Ge} = 150$ nm, and $t_{WSM} = 300$ nm or $t_{WSM} = 500$ nm, respectively. With the addition of this ultrathin metallic layer, an additional cavity is created and the nonreciprocity reaches a middle-ground between the broadband results of Fig. 4 and the high nonreciprocity contrast magnitude results of Fig. 3. Figures 6(c) and 6(d) further illustrate this tuning effect where line plots of the nonreciprocity contrast metric at $\theta = 50°$ are compared for each of the designs presented in Figs. 1(a)–1(c) when t_{Ge} is fixed to 100 nm and the WSM layer thickness is equal to either 300 nm or 500 nm, respectively. The thickness of the metallic layer can be used to tune the response. When ultrathin, some light is prevented from entering the cavity, lessening the bandwidth broadening effect. At larger thicknesses, the resulting nonreciprocity converges towards that of the monolayer design. The final trilayer design with the ultrathin metallic layer splits the difference between the other two designs and achieves a compromise between the thermal nonreciprocity bandwidth broadening and its magnitude. Finally, it is worth commenting that the refractive index of the dielectric layer does not play a substantial role in the nonreciprocal response, but low losses at mid-IR are needed to achieve the presented performance. This led us to choose Ge for the dielectric layer, which is a common semiconductor material that can be easily grown as a thin film.

Compared to other multilayer WSM designs, the nonreciprocity of our work is somewhat lower [24,26,27]. However, the nonreciprocity in these works is very narrowband and requires far more layers than the designs proposed here. More complex nanoscale patterning can be used to achieve similar bandwidth with less of a decrease in nonreciprocity [28,29], however the fabrication of WSM materials is still nascent, and such patterning may be infeasible. Comparatively, our proposed structures consist of relatively simple designs that can be feasible to fabricate via existing thin film deposition techniques. Towards this goal, recent experiments have begun to demonstrate the feasibility of growing single WSM thin films. More specifically, tantalum-arsenide (TaAs) is the first experimentally discovered [36,37] WSM material, and recent experiments have demonstrated growth of TaAs thin films via molecular beam epitaxy [38] and pulsed laser deposition [39]. Ge thin films have been deposited on metallic substrates via electron beam evaporation [40] and thin tungsten films have been grown using atomic layer deposition (ALD) [41]. Note that the ALD technique enables highly precise control of the layer thickness, making the ultrathin 5-nm-tungsten layer realization also feasible [42]. Our work presents a theoretical concept that hopefully will trigger the attention of various experimental groups that are able to experimentally realize and measure such few layer structures.

The nonreciprocity broadening effect demonstrated by these results combined with efficient operation under multiple incident angles is expected to aid in the practical realization of broadband nonreciprocal thermal emitters for efficient energy harvesting applications. More specifically, our work consists of another step toward the development of emitters for use in nonreciprocal solar thermophotovoltaics, where maintaining high solar absorption while reducing radiated thermal emission can increase the efficiency of solar thermophotovoltaic systems

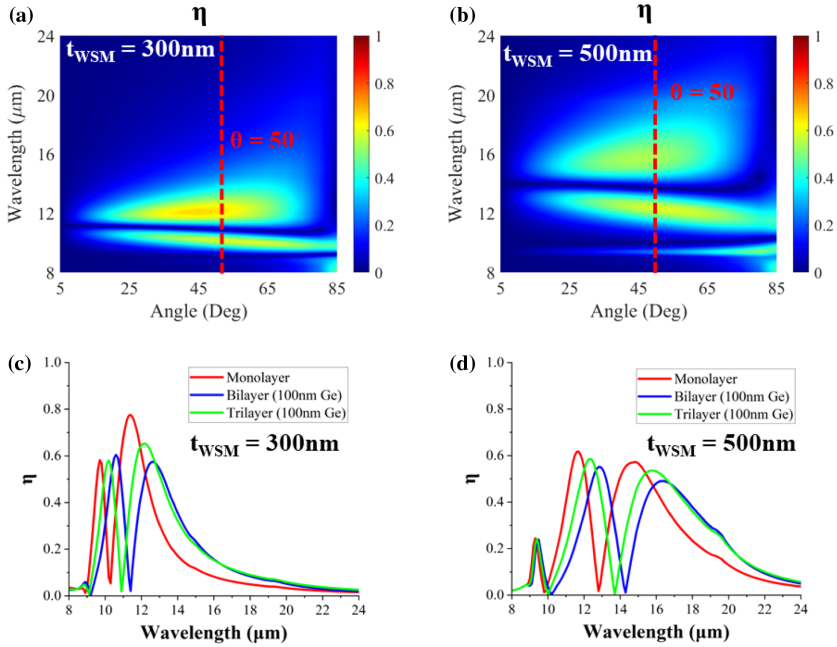

Fig. 6. (a),(b) Nonreciprocity contrast metric versus the angle and the wavelength for the trilayer structure shown in Fig. 1(c) with fixed $t_W = 5$ nm and $t_{Ge} = 150$ nm and WSM layer thicknesses of 300 nm and 500 nm, respectively. (c),(d) Line plots of the nonreciprocity contrast metric at fixed $\theta = 50°$ for each of the designs demonstrated in Figs. 1(a)–1(c) when t_{Ge} is fixed to 100 nm and the WSM layer thicknesses are equal to 300 nm and 500 nm, respectively.

to near the Landsberg limit, which is the theoretical maximum efficiency of solar energy harvesting (93.3%) [43]. Eliminating back thermal emission towards the sun in such systems will enable solar energy harvesting devices to approach this limit.

3. CONCLUSIONS

Three relatively simple-to-fabricate experimentally realized designs of broadband and wide angle nonreciprocal thermal emitters consisting of just one WSM layer were presented. The monolayer design demonstrated a trade-off relationship between the nonreciprocity contrast magnitude, and its bandwidth was based on the thickness of the WSM layer. The bilayer configuration showed additional frequency broadening of the nonreciprocal effect based on the inclusion of a dielectric spacer layer. Finally, the ability to tune the trade-off relationship between nonreciprocity contrast magnitude and bandwidth was achieved via the inclusion of an additional ultrathin metallic layer leading to a trilayer nonreciprocal thermal emitter design. The new WSM few layer structures will aid in the experimental realization of broadband and omnidirectional nonreciprocal thermal emitters. They are expected to find novel applications in emerging energy harvesting devices.

Funding. Nebraska Space Grant Consortium; National Science Foundation (2212050, 2224456); Office of Naval Research (N00014-19-1-2384).

Disclosures. The authors declare no conflicts of interest.

Data availability. Data underlying the results presented in this paper are not publicly available at this time but may be obtained from the authors upon reasonable request.

REFERENCES

1. D. G. Baranov, Y. Xiao, I. A. Nechepurenko, A. Krasnok, A. Alù, and M. A. Kats, "Nanophotonic engineering of far-field thermal emitters," Nat. Mater. **18**, 920–930 (2019).
2. A. Reicks, A. Tsubaki, M. Anderson, J. Wieseler, L. K. Khorashad, J. E. Shield, G. Gogos, D. Alexander, C. Argyropoulos, and C. Zuhlke, "Near-unity broadband omnidirectional emissivity via femtosecond laser surface processing," Commun. Mater. **2**, 36 (2021).
3. A. P. Raman, M. A. Anoma, L. Zhu, E. Rephaeli, and S. Fan, "Passive radiative cooling below ambient air temperature under direct sunlight," Nature **515**, 540–544 (2014).
4. E. Rephaeli, A. Raman, and S. Fan, "Ultrabroadband photonic structures to achieve high-performance daytime radiative cooling," Nano Lett. **13**, 1457–1461 (2013).
5. A. Butler and C. Argyropoulos, "Mechanically tunable radiative cooling for adaptive thermal control," Appl. Therm. Eng. **211**, 118527 (2022).
6. R. Sakakibara, V. Stelmakh, W. R. Chan, M. Ghebrebrhan, J. D. Joannopoulos, M. Soljačic, and I. Čelanović, "Practical emitters for thermophotovoltaics: a review," J. Photon. Energy **9**, 032713 (2019).
7. M. M. A. Gamel, H. J. Lee, W. E. S. W. A. Rashid, P. J. Ker, L. K. Yau, M. A. Hannan, and Md. Z. Jamaludin, "A review on thermophotovoltaic cell and its applications in energy conversion: issues and recommendations," Materials **14**, 4944 (2021).
8. L. Zhu and S. Fan, "Near-complete violation of detailed balance in thermal radiation," Phys. Rev. B **90**, 220301 (2014).
9. Z. Zhang and L. Zhu, "Nonreciprocal thermal photonics for energy conversion and radiative heat transfer," Phys. Rev. Appl. **18**, 027001 (2022).
10. S. A. H. Gangaraj and F. Monticone, "Drifting electrons: nonreciprocal plasmonics and thermal photonics," ACS Photonics **9**, 806–819 (2022).
11. H. Wang, H. Wu, and J.-Q. Zhou, "Nonreciprocal optical properties based on magneto-optical materials: n-InAs, GaAs and HgCdTe," J. Quant. Spectrosc. Radiat. Transf. **206**, 254–259 (2018).
12. S. A. H. Gangaraj, B. Jin, C. Argyropoulos, and F. Monticone, "Broadband field enhancement and giant nonlinear effects in terminated unidirectional plasmonic waveguides," Phys. Rev. Appl. **14**, 054061 (2020).
13. B. Zhao, Y. Shi, J. Wang, Z. Zhao, N. Zhao, and S. Fan, "Near-complete violation of Kirchhoff's law of thermal radiation with a 0.3T magnetic field," Opt. Lett. **44**, 4203–4206 (2019).
14. K. J. Shayegan, B. Zhao, Y. Kim, S. Fan, and H. A. Atwater, "Nonreciprocal infrared absorption via resonant magneto-optical coupling to InAs," Sci. Adv. **8**, 4308 (2022).
15. J. Wu, F. Wu, T. Zhao, and X. Wu, "Tunable nonreciprocal thermal emitter based on metal grating and graphene," Int. J. Therm. Sci. **172**, 107316 (2022).
16. K. Shi, Y. Xing, Y. Sun, N. He, T. Guo, and S. He, "Thermal vertical emitter of ultra-high directionality achieved through nonreciprocal magneto-optical lattice resonances," Adv. Opt. Mater. **10**, 2201732 (2022).
17. Z. Zhang and L. Zhu, "Broadband nonreciprocal thermal emission," Phys. Rev. Appl. **19**, 014013 (2023).
18. A. Ghanekar, J. Wang, C. Guo, S. Fan, and M. L. Povinelli, "Nonreciprocal thermal emission using spatiotemporal modulation of graphene," ACS Photonics **10**, 170–178 (2023).
19. T. Guo and C. Argyropoulos, "Recent advances in terahertz photonic technologies based on graphene and their applications," Adv. Photonics Res. **2**, 2000168 (2021).
20. D. L. Sounas and A. Alù, "Non-reciprocal photonics based on time modulation," Nat. Photonics **11**, 774–783 (2017).
21. S. Pajovic, Y. Tsurimaki, X. Qian, and G. Chen, "Intrinsic nonreciprocal reflection and violation of Kirchhoff's law of radiation in planar type-I magnetic Weyl semimetal surfaces," Phys. Rev. B **102**, 165417 (2020).
22. B. Zhao, C. Guo, C. A. C. Garcia, P. Narang, and S. Fan, "Axion-field-enabled nonreciprocal thermal radiation in Weyl semimetals," Nano Lett. **20**, 1923–1927 (2020).
23. J. Wu, Z. Wang, H. Zhai, Z. Shi, X. Wu, and F. Wu, "Near-complete violation of Kirchhoff's law of thermal radiation in ultrathin magnetic Weyl semimetal films," Opt. Mater. Express **11**, 4058–4066 (2021).
24. J. Wu, B. Wu, Z. Wang, and X. Wu, "Strong nonreciprocal thermal radiation in Weyl semimetal-dielectric multilayer structure," Int. J. Therm. Sci. **181**, 107788 (2022).
25. T. Li, C. Yin, and F. Wu, "Strong optical non-reciprocity in one-dimensional photonic crystal containing a Weyl semimetal-based defect," Opt. Mater.-Amsterdam **121**, 111583 (2021).
26. M. Luo, Y. Xu, Y. Xiao, and G. Yu, "Strong nonreciprocal thermal radiation by optical Tamm states in Weyl semimetallic photonic multilayers," Int. J. Therm. Sci. **183**, 107851 (2023).
27. J. Wu, Y. Sun, F. Wu, B. Wu, and X. Wu, "Enhancing nonreciprocal thermal radiation in Weyl semimetals based on optical Tamm states by integrating with photonic crystals," Waves in Random Complex Media.
28. J. Wu and Y. M. Qing, "Wide-angle and broadband nonreciprocal thermal emitter with cascaded dielectric and Weyl semimetal grating structure," Appl. Phys. Lett. **122**, 012203 (2023).
29. J. Wu, Y. Sun, B. Wu, Z. Wang, and X. Wu, "Extremely wide-angle nonreciprocal thermal emitters based on Weyl semimetals with dielectric grating structure," Case Stud. Therm. Eng. **40**, 102566 (2022).
30. J. Kischkat, S. Peters, B. Gruska, M. Semtsiv, M. Chashnikova, M. Klinkmüller, O. Fedosenko, S. Machulik, A. Aleksandrova, G. Monastyrskyi, Y. Flores, and W. T. Masselink, "Mid-infrared optical properties of thin films of aluminum oxide, titanium dioxide, silicon dioxide, aluminum nitride, and silicon nitride," Appl. Opt. **51**, 6789–6798 (2012).
31. M. A. Ordal, R. J. Bell, R. W. Alexander, L. A. Newquist, and M. R. Querry, "Optical properties of Al, Fe, Ti, Ta, W, and Mo at submillimeter wavelengths," Appl. Opt. **27**, 1203–1209 (1988).
32. T. Amotchkina, M. Trubetskov, D. Hahner, and V. Pervak, "Characterization of e-beam evaporated Ge, YbF_3, ZnS, and LaF_3 thin films for laser-oriented coatings," Appl. Opt. **59**, A40–A47 (2020).

33. C. Yang, B. Zhao, W. Cai, and Z. M. Zhang, "Mid-infrared broadband circular polarizer based on Weyl semimetals," Opt. Express **30**, 3035–3046 (2022).
34. J. Xu, J. Mandal, and A. P. Raman, "Broadband directional control of thermal emission," Science **372**, 393–397 (2021).
35. X. Wu, H. Yu, F. Wu, and B. Wu, "Enhanced nonreciprocal radiation in Weyl semimetals by attenuated total reflection," AIP Adv. **11**, 075106 (2021).
36. B. Q. Lv, H. M. Weng, B. B. Fu, X. P. Wang, H. Miao, J. Ma, P. Richard, X. C. Huang, L. X. Zhao, G. F. Chen, Z. Fang, X. Dai, T. Qian, and H. Ding, "Experimental discovery of Weyl semimetal TaAs," Phys. Rev. X **58**, 675–676 (2015).
37. S.-Y. Xu, I. Belopolski, N. Alidoust, *et al.*, "Discovery of a Weyl fermion semimetal and topological Fermi arcs," Science **349**, 613–617 (2015).
38. J. Sadowski, J. Z. Domagała, W. Zajkowska, S. Kret, B. Seredyński, M. Gryglas-Borysiewicz, Z. Ogorzałek, R. Bożek, and W. Pacuski, "Structural properties of TaAs Weyl semimetal thin films grown by molecular beam epitaxy on GaAs(001) substrates," Cryst. Growth Des. **22**, 6039–6045 (2022).
39. S. Li, Z. Lin, W. Hu, D. Yan, F. Chen, X. Bai, B. Zhu, J. Yuan, Y. Shi, K. Jin, H. Weng, and H. Guo, "Exploration of growth conditions of TaAs Weyl semimetal thin film using pulsed laser deposition," Chin. Phys. B **32**, 047103 (2023).
40. K. Kim, G. Radhakrishnan, R. Droopad, and A. Goyal, "Single-crystal-like germanium thin films on large-area, compliant, light-weight, flexible, single-crystal-like substrates," PNAS Nexus **1**, pgac098 (2022).
41. M. Lee, R. Hidayat, D. K. Nandi, T. H. Kim, Y. Kim, S. Kim, W.-J. Lee, and S.-H. Kim, "Atomic layer deposition of tungsten and tungsten-based compounds using WCl_5 and various reactants selected by density functional theory," Appl. Surf. Sci. **563**, 150373 (2021).
42. J. A. Oke and T.-C. Jen, "Atomic layer deposition and other thin film deposition techniques: from principles to film properties," J. Mater. Res. Technol. **21**, 2481–2514 (2022).
43. S. J. Ghalekohneh and B. Zhao, "Nonreciprocal solar thermophotovoltaics," Phys. Rev. Appl. **18**, 034083 (2022).